Journal of Thermal Analysis and Calorimetry (2020) 141:2061–2079
https://doi.org/10.1007/s10973-019-08963-6

Mixed convection in a trapezoidal enclosure filled with two layers of nanofluid and porous media with a rotating circular cylinder and a sinusoidal bottom wall

Ahmed Kadhim Hussein[1] · Hameed K. Hamzah[1] · Farooq H. Ali[1] · Lioua Kolsi[2,3]

Received: 19 June 2019 / Accepted: 25 October 2019 / Published online: 16 November 2019

Abstract
The laminar two-dimensional mixed convection in a trapezoidal enclosure with a rotating inner circular cylinder and a sinusoidal bottom wall is studied numerically. The fluid inside the enclosure is a CuO–water nanofluid layer in the top space of it, while the bottom space includes a CuO–water nanofluid saturated with a porous medium. Both the right and left sidewalls are assumed adiabatic, while the bottom and the top walls of the enclosure are maintained, respectively, at the hot and cold temperatures. The dimensionless governing equations are expressed for velocity and temperature formulation and modeled by using COMSOL code based on the Galerkin finite element method. Parametric studies on the effects of various significant parameters such as Rayleigh number, Darcy number, the inner cylinder radius, the porous layer thickness, the angular rotational velocity, the solid volume fraction and the number of undulations on the flow and thermal fields together with the heat transfer rate have been performed. The highest value of the stream function for ($\mathrm{Ra}=10^3$ and $\mathrm{Ra}=10^5$) is seen at ($R=0.2$ and $S=0.2$). The same thing is observed, when the bottom wall is considered wavy. For ($\mathrm{Ra}=10^3$ and $N=0$) and ($0.5\leq S\leq 0.8$), it can be seen that as the inner cylinder radius increases from ($R=0.1$) to ($R=0.3$), the stream function values increase continuously. It is found that the average Nusselt number increases as the Rayleigh and Darcy numbers, the solid volume fraction, inner cylinder radius and the angular rotational velocity of the cylinder increase, while it decreases as the porous layer thickness and the number of undulations increase. Comparisons with previously published numerical works are performed, and good agreements between the results are observed.

Keywords Mixed convection · Nanofluid · Trapezoidal enclosure · Porous media · Rotating cylinder · Sinusoidal wall

List of symbols

c_p	Heat capacitance (J kg^{-1} °C^{-1})
Da	Darcy number
g	Gravitational acceleration (m s^{-2})
k_f	Thermal conductivity of the fluid (W m^{-1} °C^{-1})
L	Height and width of the trapezoidal enclosure (m)
Nu	Nusselt number
N	Number of undulations
P	Dimensionless pressure
p	Pressure (N m^{-2})
Pr	Prandtl number
R	Dimensionless radius of the inner cylinder
r	Radius of the inner cylinder (m)
Ra	Rayleigh number
Re	Reynolds number
Ri	Richardson number
S	Porous layer thickness (m)
T	Temperature (°C)
U	Dimensionless velocity component in x-direction
u	Dimensional velocity component in x-direction (m s^{-1})
V	Dimensionless velocity component in y-direction
v	Dimensional velocity component in y-direction (m s^{-1})
w	Width of the trapezoidal enclosure (m)
X	Dimensionless coordinate in horizontal direction
x	Cartesian coordinate in horizontal direction (m)

✉ Lioua Kolsi
lioua_enim@yahoo.fr

[1] College of Engineering, Mechanical Engineering Department, University of Babylon, Babylon City, Hilla, Iraq

[2] College of Engineering, Mechanical Engineering Department, University of Ha'il, Ha'il City, Saudi Arabia

[3] Laboratoire de Métrologie et des Systèmes Énergétiques, École Nationale d'Ingénieurs, University of Monastir, Monastir, Tunisia

Y Dimensionless coordinate in vertical direction
y Cartesian coordinate in vertical direction (m)

Greek symbols

α Thermal diffusivity ($m^2\ s^{-1}$)
β Volumetric thermal expansion coefficient (K^{-1})
θ Dimensionless temperature distribution
φ Solid volume fraction
ε Porosity
ζ Amplitude of the wavy wall
Ω Dimensionless angular rotational velocity
ω Angular rotational velocity (rad s^{-1})
ν Kinematic viscosity ($m^2\ s^{-1}$)
ρ Density (kg m^{-3})
μ Dynamic viscosity (kg $m^{-1}\ s^{-1}$)
Ψ Dimensionless stream function
λ Permeability of the porous medium (m^2)

Subscripts

ave Average
c Cold
eff Effective
fl Base fluid
h Hot
loc Local
Max Maximum
Min Minimum
na Nanofluid particle
o Center of enclosure
po Porous medium
so Solid particles

Introduction

Nanofluid is a scientific term which was firstly used by Choi [1] in 1995 during his work in Argonne National Laboratory in the USA. This term refers to a solid–liquid composite material which consists of solid nanoparticles with a size of 1–100 nm suspended in a traditional liquid [2]. The main function of inventing the nanofluids is to overcome the extremely poor thermal conductivity of the most famous traditional liquids like water, engine oil and ethylene glycol [3]. Due to the amazing properties of the nanofluid, it was attracted a high interest from the research community especially in the last 10 years. This is of course can be go back to the huge applications of it in many important fields such as in solar collectors and stills, compact heat exchangers, microelectronics, food and agricultural technologies, automotive cooling system, oil industry, water purification, heat pipes and lubrication oils [4]. For an extra information about the nanofluid, the reader can be returned to a set of many significant review papers such as Hussein [5, 6], Hussein et al. [7] and very recently by Mahian et al. [8, 9]. From the another side, the mixed convection heat transfer is a very important phenomenon which received an intense attention in the last decades due to their wide applications in the industry and the real life. Some of these applications include building design, solar heating and cooling, air conditioning, material processing, fire control in buildings and electronic cooling [10–13]. Therefore, the mixed convection can be used as an effective and an efficient tool to enhance the heat transfer rate. The mixed convection comes from the combined simultaneous effect of the natural convection and the forced convection. The first one comes from the buoyancy force which caused by the temperature difference between the hot and cold surfaces, while the second one comes from the mechanical effect or some times called the shear force. There are many examples of the mechanical effect such as fans, rotating cylinder and the lid-driven wall(s). These important and practical applications motivated many authors to investigate the mixed convection in enclosures especially in the last 2 years. The first group of researchers studied this phenomenon in enclosures filled with classical fluid. Examples of these researches include Hussein and Hussain [14], Saha et al. [15], Gangawane et al. [16], Chakravarty et al. [17], Taghizadeh and Asaditaheri [18] and Alsabery et al. [19]. The second group of them were investigated the mixed convection in classical or complicated enclosures filled with nanofluid under different situations. The MHD mixed convection in a lid-driven square enclosure with a thin center heater and filled with Ag–water nanofluid was investigated numerically by Mahalakshmi et al. [20]. The finite volume method and SIMPLE algorithm with a power-law scheme were utilized to solve the governing equations. The enclosure was isothermally cooled at the vertical oppositely moving sidewalls, whereas an isothermal heat source was maintained at the bottom wall. The remaining parts of the bottom wall together with the top wall were assumed adiabatic. The center heater was kept at both horizontal and vertical positions in the enclosure. The results were illustrated for a wide range of the Richardson number ($0.01 \le \mathrm{Ri} \le 100$), Hartmann number ($0 \le \mathrm{Ha} \le 50$), heater length ($0.25 \le \Gamma \le 0.75$) and solid volume fraction of nanoparticles ($0 \le \phi \le 0.09$). They concluded that the heat transfer rate was enhanced by increasing the Grashof number, solid volume fraction and the heater length, while it was decreased by increasing the Hartmann number. The double-diffusive mixed convection in an inclined lid-driven enclosure filled with a water-saturated nanofluid in the presence of the internal heat generation was investigated numerically by Yu et al. [21]. Both the left and right sidewalls of the enclosure were assumed fixed and heated as a sine wave, while the top and bottom walls were assumed adiabatic and moved in an opposite direction. It was found

that both the average Nusselt and Sherwood numbers were varied periodically inside the enclosure. Zhou et al. [22] utilized the lattice Boltzmann method (LBM) to perform a numerical study of the mixed convection in a cubic cavity filled with alumina–water nanofluid. The left sidewall of the cavity was kept at a uniform or non-uniform hot temperature, while the right one was considered cold. Both of them were considered moving in an upward or downward direction. All the remaining walls were assumed insulated. They deduced that the heat transfer was enhanced by decreasing the Richardson number and increasing the solid volume fraction. Mamourian et al. [23] investigated numerically the mixed convection optimization with an entropy generation in a square lid-driven cavity with a wavy surface and filled with Cu–water nanofluid by using the Taguchi approach. The effects of the Richardson number, solid volume fraction and wavelengths of the wavy wall on the flow and thermal fields together with the Nusselt number were investigated. They concluded that the mean Nusselt number was decreased by increasing the Richardson number and the solid volume fraction. Cho [24] investigated numerically the mixed convection and the entropy generation in a lid-driven wavy-wall cavity filled with a copper–water nanofluid. The hot left sidewall of the cavity was considered lid-driven and flat, while the right one was assumed stationary, cold and wavy. The top and bottom walls were assumed adiabatic and flat. He concluded that the increase in the solid volume fraction, amplitude of the wavy surface, Richardson and Reynolds numbers led to increase in the mean Nusselt number and the total entropy generation. Pal et al. [25] carried out a numerical study about the conjugate mixed convection and the entropy generation of Cu–water nanofluid in a lid-driven enclosure with a thick wavy heated bottom wall. The adiabatic top wall was assumed slide to the right, while both the left and right sidewalls were maintained at a constant cold temperature. The effects of the wavy fluid–solid interface, solid-to-fluid thermal conductivity ratio and nanoparticle volume fraction on the heat transfer characteristics were analyzed for various values of the Richardson number. They deduced that the effect of the wavy surface became significant when the solid conductivity was equivalent to the fluid conductivity. Alsabery et al. [26] performed a numerical study by using the Galerkin finite element method of the mixed convection and the entropy generation in a wavy-walled cavity filled with Al_2O_3–water nanofluid and involved a rotating conductive cylinder. Both the top and bottom walls were considered adiabatic, except the heat source segment located at the bottom wall. The vertical walls of the cavity were assumed cooled and wavy. The effects of the Rayleigh number, number of undulations, solid volume fraction, the heat source length and the angular rotational velocity on streamline and isotherm contours together with the Bejan and Nusselt numbers were analyzed. They concluded that the Nusselt number was improved by increasing the heat source length and the solid volume fraction. Also, they found that the rotating cylinder was enhanced the heat exchange rate for Rayleigh number less than 5×10^5. Very recently, Alsabery et al. [27] carried out a computational study of the transient mixed convection in a double lid-driven wavy cavity with a centered solid circular cylinder by using the non-homogeneous nanofluid model. The cavity was filled with the Al_2O_3–water nanofluid. The top wall of the cavity was assumed stationary, wavy and adiabatic, while the bottom wall of it was kept flat, stationary and adiabatic also. Both the hot left and the cold right vertical walls were considered moving upward in the positive and negative directions. The results indicated that the increase in the average Nusselt number was connected by the moving parameter. Moreover, as the inner cylinder diameter and the number of undulations were increased, the thermal transmission intensity was diminished. Alsabery et al. [28] performed a numerical study of the conjugate mixed convection in a double lid-driven square cavity with a square solid inner body. The cavity was filled with Al_2O_3–water nanofluid based on Buongiorno's two-phase model. The hot bottom wall of the cavity was moved to the left, while the cold top wall of it was moved to the right. They presented the results for a wide range of the Richardson number ($0.01 \le \mathrm{Ri} \le 100$), Reynolds number ($1 \le \mathrm{Re} \le 500$), the size of the inner body ($0.1 \le D \le 0.7$), the solid volume fraction ($0 \le \phi \le 0.04$), the thermal conductivity of the inner body ($0.01 \le k_w \le 1.95\ \mathrm{W\ m^{-1}\ ^oC^{-1}}$) and four cases of the inner body location. It was found that the big size of the inner body was improved the heat transfer for high Richardson and Reynolds numbers. Nayak et al. [29] studied numerically the effects of nanoparticles dispersion on the mixed convection and the entropy generation in a skewed enclosure filled with Cu–water nanofluid. The insulated upper wall was assumed moved horizontally to the right, while both the stationary left and right sidewalls were maintained at a constant hot and cold temperature, respectively. With respect to the lower wall, it was considered insulated and stationary also. The effects of the Brownian diffusion, solid volume fraction, nanoparticles size and thermophoretic diffusion on the mixed convection were studied. They concluded that the Brownian motion and thermophoresis had a negligible effect on the mixed convection and the entropy generation inside the cavity. Very recently, Garmroodi et al. [30] numerically simulated the MHD mixed convection of copper–water nanofluid inside a lid-driven square cavity in the presence of multiple adiabatic rotating cylinders with four different configurations. A two-phase mixture model was adapted to simulate the nanofluid flow

and the heat transfer. The upper wall of the cavity was assumed lid-driven and cold, while the lower wall was considered hot and fixed. Both the left and right sidewalls were assumed stationary and thermally insulated. It was found that the vertical arrangement of the cylinders led to a maximum heat transfer rate inside the cavity. Other useful references about the mixed convection in cavities filled with nanofluid can be found in [31–35].

From the another side, limited researchers studied the mixed convection in an enclosure filled a nanofluid saturated with a porous medium. Rajarathinam et al. [36] investigated numerically the mixed convection of copper–water nanofluid in an inclined fluid-saturated porous cavity. Three different cases depended on the direction of moving wall(s) were considered. The results were presented for various parameters such as the solid volume fraction, Darcy and Richardson numbers, inclination angle and the direction of moving wall(s). It was found that the heat transfer rate was enhanced by decreasing the Richardson number and increasing the inclination angle and the Darcy number. Astanina et al. [37] investigated numerically the mixed convection of alumina–water nanofluid in a lid-driven cavity which had two different porous layers located on the hot bottom wall. The upper wall of the cavity was considered lid-driven and maintained at a constant cold temperature. The vertical sidewalls were assumed adiabatic. The results were illustrated for a wide range of the Richardson number ($0.01 \le \mathrm{Ri} \le 10$), Darcy number for the first porous layer ($10^{-7} \le \mathrm{Da} \le 10^{-3}$), porous layers thickness ($0.1 \le \delta \le 0.3$) and nanoparticles volume fraction of ($0 \le \phi \le 0.04$), while the Reynolds number, Prandtl number and Darcy number for the second porous layer were considered constant at $\mathrm{Re} = 100$, $\mathrm{Pr} = 6.82$, $\mathrm{Da} = 10^{-5}$, respectively. It was found that the addition of nanoparticles was reduced the heat transfer in the mixed and forced convection regimes, while an opposite behavior was noticed in the natural convection regime. Very recently, Xu et al. [38] presented an excellent review about the convection heat transfer of the nanofluids saturated with a porous medium. On the same manner, a very limited paper which deals with the mixed convection problem in a trapezoidal enclosure filled a nanofluid. Kareem et al. [39] studied numerically the effect of using four types of nanofluids (Al_2O_3, CuO, SiO_2 and TiO_2 with pure water) on the mixed convection in a lid-driven inclined trapezoidal enclosure. Both the vertical sidewalls of the enclosure were assumed adiabatic. The upper wall was considered cold and moved either in a positive or negative x-direction, while the hot lower wall was considered stationary. The results were computed for the Richardson number ($0.1 \le \mathrm{Ri} \le 10$), Reynolds number ($100 \le \mathrm{Re} \le 1200$), nanoparticle diameter ($25 \le d_p \le 70$ nm), the solid volume fraction ($0.01 \le \phi \le 0.04$), the rotational angles ($30° \le \Phi \le 60°$), enclosure aspect ratios ($0.5 \le A \le 2$) and inclination sidewalls angles ($30° \le \gamma \le 60°$). They concluded that the Nusselt number was increased by increasing the solid volume fraction and the aspect ratio, while it was decreased by increasing both the rotational and inclination angles and the nanoparticle diameter. The MHD mixed convection in a lid-driven trapezoidal cavity filled with a copper–water nanofluid was carried out by Chamkha and Ismael [40]. Both the horizontal walls were considered adiabatic and stationary, while the cold left and the hot right vertical walls were assumed fixed and moved upward or downward, respectively. The streamlines, isotherms and Nusselt number results were illustrated for a wide range of the Hartmann number ($0 \le \mathrm{Ha} \le 100$), Richardson number ($0.01 \le \mathrm{Ri} \le 10$), the inclination angle of the cavity sidewalls ($\phi = 66°$, 70° and 80°) and the solid volume fraction ($0 \le \phi \le 0.05$). It was found that the average Nusselt number was maximum at higher inclination angles of the cavity sidewalls. Selimefendigil and Oztop [41] carried out a numerical study of the MHD mixed convection in a lid-driven trapezoidal cavity filled with alumina–water nanofluid for various electrical conductivity models. Both the fixed left and right sidewalls of the cavity were assumed thermally insulated. The hot bottom wall of the cavity was assumed fixed, while the cold top wall of it was moved to

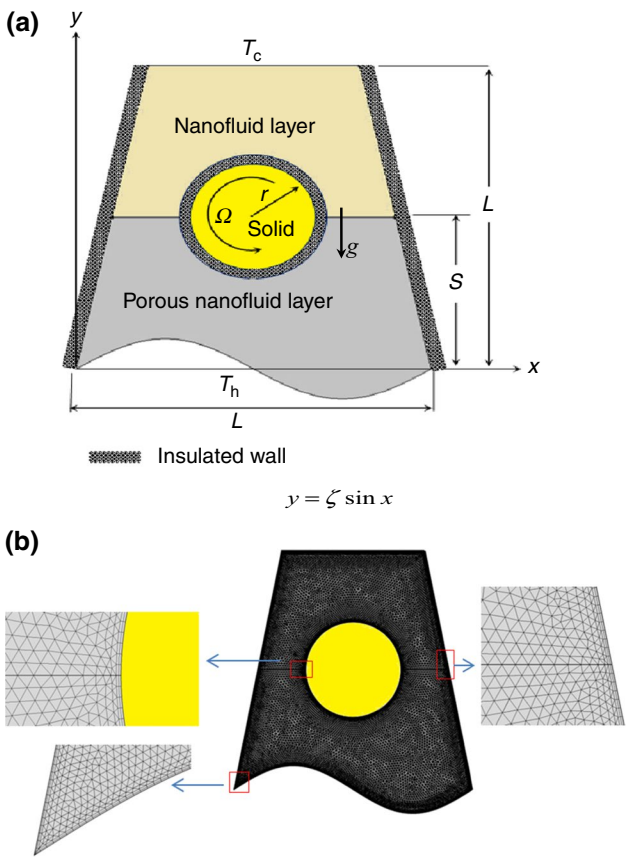

Fig. 1 **a** Schematic diagram of the present problem, **b** Mesh distribution of the computational domain

Table 1 Thermo-physical properties of base fluid (pure water) and (CuO) nanoparticles

Properties	Pure water	CuO
c_p/J kg^{-1} k^{-1}	4179	540
k/W m^{-1} k^{-1}	0.6	18
ρ/kg m^{-3}	997.1	6500
β/k^{-1}	21×10^{-5}	0.85×10^{-5}
d_p/nm	0.384	29

the right at a uniform velocity. Numerical computations were performed for various electrical conductivity models and different values of the Hartmann number ($0\le Ha\le 40$), Richardson number ($0.01\le Ri\le 25$), magnetic field inclination angle ($0^\circ\le\gamma\le 90^\circ$) and the solid volume fraction ($0\le\phi\le 0.03$). They concluded that as the solid volume fraction increased, the differences between average Nusselt numbers were increased for various electrical conductivity models. Other useful references about the mixed convection and the nanofluid can be found in [42–54]. Therefore, it can be concluded from the previous recent literature review and according also to the authors' best experience in this field that no available paper at all deals with the mixed convection phenomena in a trapezoidal enclosure with a sinusoidal bottom wall which filled with two layers of nanofluid and porous media and including a rotating circular cylinder.

Mathematical modeling

Governing equations and geometrical configuration

Figure 1a, b shows, respectively, a schematic diagram and the mesh distribution of a two-dimensional trapezoidal enclosure of height and width (L) together with the important geometric parameters. The fluid inside the enclosure is a CuO–water nanofluid layer in the top space of it, while the bottom space includes a CuO–water nanofluid saturated with a porous medium. Both the right and left sidewalls are assumed thermally insulated, while the bottom and the top walls of the enclosure are maintained, respectively, at the hot and cold temperatures. An adiabatic rotating circular cylinder is placed in the center of the enclosure and rotates about its centroidal axis. The nanofluid is assumed to be incompressible, and the flow is assumed to be two-dimensional, laminar and steady. It is assumed that the base fluid (i.e., water) and nanoparticles are in a thermal equilibrium state. The thermo-physical properties of the base fluid and nanoparticles are included in Table 1. The Rayleigh number is varied as ($Ra=10^3$, 10^5 and 10^6), the Darcy number is varied as ($10^{-5}\le Da\le 10^{-2}$), the inner cylinder radius is varied as ($R=0.1$, 0.2 and 0.3), the porous layer thickness (S) is varied as ($S=0.2$, 0.5 and 0.8), the angular rotational velocity is varied as ($0\le\Omega\le 6000$), while the solid volume fractions (ϕ) are varied as ($0\le\phi\le 0.06$) and the number of undulations are varied as ($1\le N\le 3$).

The thermo-physical properties of both the base fluid and nanofluids are assumed to be constant except for the density variation, which is modeled using Boussinesq model. Under these assumptions, the dimensional governing continuity, momentum and energy equations are, respectively, expressed as:

$$\frac{\partial u_{\mathrm{na,po}}}{\partial x}+\frac{\partial v_{\mathrm{na,po}}}{\partial y}=0 \tag{1}$$

$$\frac{\rho_{\mathrm{na}}}{\epsilon^2}u_{\mathrm{na,po}}\frac{\partial u_{\mathrm{na,po}}}{\partial x}+\frac{\rho_{\mathrm{na}}}{\epsilon^2}v_{\mathrm{na,po}}\frac{\partial u_{\mathrm{na,po}}}{\partial y}= -\frac{\partial p_{\mathrm{na,po}}}{\partial x}+\frac{\mu_{\mathrm{na}}}{\epsilon}\left(\frac{\partial^2 u_{\mathrm{na,po}}}{\partial x^2}+\frac{\partial^2 u_{\mathrm{na,po}}}{\partial y^2}\right)-\sigma\left(\frac{\mu_{\mathrm{na}}}{\lambda_{\mathrm{po}}}u_{\mathrm{po,na}}\right) \tag{2}$$

$$\frac{\rho_{\mathrm{na}}}{\epsilon^2}u_{\mathrm{na,\,po}}\frac{\partial v_{\mathrm{na,\,po}}}{c}+\frac{\rho_{\mathrm{na}}}{\epsilon^2}v_{\mathrm{na,\,po}}\frac{\partial v_{\mathrm{na,\,po}}}{\partial y} =-\frac{\partial \rho_{\mathrm{na,\,po}}}{\partial y}+\frac{\mu_{\mathrm{na}}}{\epsilon^2}\left(\frac{\partial^2 v_{\mathrm{na,\,po}}}{\partial x^2}+\frac{\partial^2 v_{\mathrm{na,\,po}}}{\partial y^2}\right) +(\rho\beta)_{\mathrm{na,\,po}}g(T-T_{\mathrm{c}})-\sigma\left(\frac{\mu_{\mathrm{na}}}{\lambda_{\mathrm{po}}}v_{\mathrm{po,\,na}}\right) \tag{3}$$

$$u_{\mathrm{po,na}}\frac{\partial T_{\mathrm{na,po}}}{\partial x}+v_{\mathrm{po,na}}\frac{\partial T_{\mathrm{na,pa}}}{\partial y}=-\frac{k_{\mathrm{na,po}}}{(\rho c_{\mathrm{p}})_{\mathrm{na}}}\left(\frac{\partial^2 T_{\mathrm{na,po}}}{\partial x^2}+\frac{\partial^2 T_{\mathrm{na,po}}}{\partial y^2}\right). \tag{4}$$

The set of Eqs. (1–4) was transferred to a dimensionless form after considering the following specifications:

1. Dimensionless scales

$$X,Y=\frac{x,y}{L},U,V=\frac{(u,v)L}{\alpha_{\mathrm{fl}}},\theta=\frac{T-T_{\mathrm{c}}}{T_{\mathrm{h}}-T_{\mathrm{c}}},$$
$$P=\frac{(p+\rho_{\mathrm{ofl}}g_{\mathrm{y}})L^2}{\rho_{\mathrm{fl}}\alpha_{fl}^2},\ R=\frac{r}{L},\ \Omega=\frac{\omega L^2}{\alpha_{\mathrm{fl}}}$$

2. Dimensionless numbers

$$\mathrm{Pr}=\frac{\nu_{\mathrm{fl}}}{\alpha_{\mathrm{fl}}}(\text{Prandtl number}),\ \mathrm{Da}=\frac{\lambda}{L^2}(\text{Darcy number}),$$
$$\mathrm{Ra}=\frac{g\beta_{\mathrm{fl}}(T_{\mathrm{h}}-T_{\mathrm{c}})L^3}{\alpha_{\mathrm{fl}}\nu_{\mathrm{fl}}}(\text{Rayleigh number}),$$
$$\mathrm{Re}=\frac{\omega rL}{\nu_{\mathrm{fl}}}(\text{Reynolds number}),\ \mathrm{Ri}=\frac{\mathrm{Ra\,Pr}}{\Omega^2R^2}(\text{Richardson number})$$

The density and the heat capacity of CuO–water nanofluid are determined as follows:

$$\rho_{na} = (1-\phi)\rho_{fl} + \phi\rho_{so}, \left(\rho C_p\right)_{na} = (1-\phi)\left(\rho C_p\right)_{fl} + \phi\left(\rho C_p\right)_{so} \tag{5}$$

The coefficient of thermal expansion of CuO–water nanofluid is defined as:

$$(\rho\beta)_{na} = (1-\phi)_{fl} + \phi(\rho\beta)_{so} \tag{6}$$

The viscosity and the thermal conductivity of CuO–water nanofluid are expressed as:

$$\mu_{na} = \frac{\mu_{fl}}{\left(1-\emptyset\right)^{2.5}}; \frac{k_{na}}{k_{fl}} = \frac{k_{so} + 2k_{fl} - 2\emptyset\left(k_{fl} - k_{so}\right)}{k_{so} + 2k_{fl} + 2\emptyset\left(k_{fl} - k_{so}\right)} \tag{7}$$

Then, the dimensionless form of Eqs. (1–4) is given by:

Continuity equation:

$$\frac{\partial U_{na,p}}{\partial X} + \frac{\partial V_{na,po}}{\partial Y} = 0 \tag{8}$$

X-component momentum equation:

$$U_{na,po}\frac{\partial U_{na,po}}{\partial X} + V_{na,po}\frac{\partial U_{na,po}}{\partial Y} = -\frac{\rho_{fl}}{\rho_{na}}\varepsilon^2\frac{\partial P_{na,po}}{\partial X} + \frac{\rho_{fl}}{\rho_{na}}\frac{\mu_{na}}{\mu_{fl}}\varepsilon\,\mathrm{Pr}\left(\frac{\partial^2 U_{na,po}}{\partial X^2} + \frac{\partial^2 U_{na,po}}{\partial Y^2}\right) - \frac{\rho_{fl}}{\rho_{na}}\frac{\mu_{na}}{\mu_{fl}}\sigma\varepsilon^2\frac{\mathrm{Pr}}{\mathrm{Da}}U_{na,po} \tag{9}$$

Y-component momentum equation:

$$U_{na,po}\frac{\partial V_{na,po}}{\partial X} + V_{na,po}\frac{\partial V_{na,po}}{\partial Y} = -\frac{\rho_{fl}}{\rho_{na}}\varepsilon^2\frac{\partial P_{na,po}}{\partial Y} + \frac{\rho_{fl}}{\rho_{na}}\frac{\mu_{na}}{\mu_{fl}}\varepsilon\,\mathrm{Pr}\left(\frac{\partial^2 V_{na,po}}{\partial X^2} + \frac{\partial^2 V_{na,po}}{\partial Y^2}\right) - \frac{\rho_{fl}}{\rho_{na}}\frac{\mu_{na}}{\mu_{fl}}\sigma\varepsilon^2\frac{\mathrm{Pr}}{\mathrm{Da}}V_{na,po} + \frac{(\rho\beta)_{na}}{\rho_{nf}\beta_{fl}}\varepsilon^2\mathrm{RaPr}\theta \tag{10}$$

Energy equation:

$$U_{na,po}\frac{\partial\theta_{na,po}}{\partial X} + V_{na,po}\frac{\partial\theta_{na,po}}{\partial Y} = \frac{\alpha_{eff}}{\alpha_{fl}}\left(\frac{\partial^2\theta_{na,po}}{\partial X^2} + \frac{\partial^2\theta_{na,po}}{\partial Y^2}\right) \tag{11}$$

It is useful to mention that the movement within the porous layer follows the Darcy–Brinkman approach. The porosity of the porous layer is taken as ($\varepsilon = 0.398$), while the thermal conductivity is taken as ($k_{po} = 0.845$ W/m.K). The values of ε, σ and α_{eff} for two layers of the nanofluid and the porous medium are given by:

For nanofluid layer ($\varepsilon = 1$, $\sigma = 0$, $\alpha_{eff} = \alpha_f$,)

For porous medium layer ($\varepsilon = \varepsilon$, $\sigma = 1$, $\alpha_{eff} = \alpha_{eff}$)

The flow pattern through the enclosure was described by streamlines which are determined by the following equation:

$$\frac{\partial^2\Psi_{na,po}}{\partial X^2} + \frac{\partial^2\Psi_{na,po}}{\partial Y^2} = \frac{\partial U_{na,po}}{\partial Y} - \frac{\partial V_{na,po}}{\partial X}. \tag{12}$$

Boundary conditions and Nusselt number computation

The boundary conditions of the present study can be expressed as follows:

1. For the top horizontal wall

$$U_{na} = V_{na} = \Psi_{na} = 0, \quad T = T_c \rightarrow \theta = 0$$

2. For the bottom horizontal wall

$$U_{po} = V_{po} = \Psi_{po} = 0, \quad T = T_h \rightarrow \theta = 1$$

3. For the left and right inclined walls

$$U_{na,po} = V_{na,po} = \Psi_{na,po} = 0, \ \frac{\partial\theta_{na,po}}{\partial n} = 0$$

4. Around the rotating cylinder surface

$$U_{na,po} = \frac{\partial\Psi_{na,po}}{\partial Y} = U_o\frac{\left(Y - Y_o\right)}{R} = \Omega\left(Y - Y_o\right)$$

$$V_{na,po} = \frac{\partial\Psi_{na,po}}{\partial X} = U_o\frac{\left(X_o - X\right)}{R} = \Omega\left(X_o - X\right)$$

$$\left(\frac{\partial\theta}{\partial n}\right)_{na} = \left(\frac{\partial\theta}{\partial n}\right)_{po} = 0$$

5. On the interface wall between the nanofluid and the porous media layers

$$U_{na} = U_{po}, \ V_{na} = V_{po}$$

$$\left(\frac{\partial U}{\partial Y} + \frac{\partial V}{\partial x}\right)_{na} = \left(\frac{\partial U}{\partial Y} + \frac{\partial V}{\partial X}\right)_{po}$$

$$\left(\frac{\partial\theta}{\partial Y}\right)\text{nano layer} = \left(\frac{k_{eff}}{k_f}\frac{\partial\theta_{po}}{\partial Y}\right)\text{porous layer},$$

$$\theta_{na} = \theta_{po}$$

The local and average Nusselt numbers along the sinusoidal bottom hot wall are calculated from the following two equations:

$$\mathrm{Nu}_{loc} = -\frac{k_{eff}}{k_{fl}}\frac{\partial\theta_{po}}{\partial Y}\Bigg\}_{Y=0} \tag{13}$$

$$\mathrm{Nu}_{ave} = \int_0^1 \mathrm{Nu}_{loc}\mathrm{d}X. \tag{14}$$

The amplitude of the wavy wall

The wavy bottom wall is considered sinusoidal and its amplitude is given by:

$$y = \zeta \sin x \tag{15}$$

where ζ is considered constant as ($\zeta = 0.1$).

Numerical method and verification

The governing dimensionless equations [i.e., Eqs. (8–11)] are solved numerically by using Galerkin finite elements approach to determine the stream function and the dimensionless temperature distribution inside the enclosure. Lagrange finite elements were employed to discretize the velocity in the X and Y directions, pressure and temperature through the domain. The variables within the domain are divided into non-flapping zones through employing initiation functions. After replacing the variables into the dimensional governing equation, residual will product and it resolved to reinforce equals to zero up the computational region as:

$$\int_{\tau} WD\mathrm{d}\tau \tag{16}$$

where (W) expressed the mass function in Galerkin approach; it is selected from the equivalently arranged functions called the trial function. The production is so that each node on the element have a nonlinear residual equation where calculated by using the Newton–Raphson scheme. The iteration of the present study is assumed to be convergence solution when the corresponding error of each variable equals or less than 10^{-6}. Non-homogeneous distribution, triangular mesh element is chosen to mesh both nanofluid and the porous medium domains. To check the grid sensitivity for the present model, different types of mesh size, number of elements, boundary elements and time elapsed to solve were achieved as shown in Table 2. An average Nusselt number of the bottom hot wall in the case of ($S = 0.5$, $R = 0.2$, $\mathrm{Ra} = 10^5$, $\Omega = 3000$, $\varphi = 0.02$ and $\mathrm{Da} = 5 \times 10^{-5}$) was considered. The less percentage error is selected which equals to (−0.064) at an extremely fine mesh with number of elements equals to (22,251) and boundary elements equals to (837), and time elapsed was about 22 s. Table 2 shows an increase in the time required to solve the problem with increasing number of mesh elements. This is due to the increase in the number of nodes in order to reach the accurate solution. To provide the accuracy of the numerical approach of the present code, the fluid flow structure represents by streamline contours, the heat transfer represents by isotherm contours and the average Nusselt number is computed and compared with the previous numerical study performed by Selimefendigil et al. [42] as shown in Fig. 2 and Table 3. It is noticeable that there is a very good agreement between the two results. Therefore, the results of the present numerical code are verified by this comparison.

Table 2 Grid sensitivity check for the case ($S = 0.5$, $R = 0.2$, $\mathrm{Ra} = 10^5$, $\Omega = 3000$, $\varphi = 0.02$, $\mathrm{Da} = 5 \times 10^{-5}$)

Mesh size	Mesh elements	Boundary elements	CPU time/s	$\overline{\mathrm{Nu}}$	Error%
Normal	1546	178	7	1.5749	–
Fine	2319	223	9	1.5802	0.33
Finer	6826	438	11	1.5507	−1.9
Extra fine	19,033	837	20	1.5473	−0.219
Extremely fine	22,251	837	22	1.5463	−0.064

Results and discussion

In this section, the results obtained from the numerical simulation of the two-dimensional laminar mixed convection in a trapezoidal enclosure filled with two layers of nanofluid and porous media with a rotating circular cylinder and a sinusoidal bottom wall were presented and discussed in more details. The effects of the Rayleigh number (Ra), the Darcy number (Da), the inner cylinder radius (R), the porous layer thickness (S), the solid volume fraction (ϕ), the angular rotational velocity (Ω) and the number of undulation (N) on the flow and thermal fields together with the average Nusselt number have been illustrated and discussed also. In the present work, the solid volume fraction (ϕ) is varied as ($0 \le \phi \le 0.06$), the Rayleigh number is varied as ($10^3 \le \mathrm{Ra} \le 10^6$), the Darcy number is varied as ($10^{-5} \le \mathrm{Da} \le 10^{-2}$), the inner cylinder radius is varied as ($R = 0.1$, 0.2 and 0.3), the angular rotational velocity is varied as ($0 \le \Omega \le 6000$), the porous layer thickness (S) is varied as ($S = 0.2$, 0.5 and 0.8) and the number of undulations is varied as ($1 \le N \le 3$).

Effects of the inner cylinder radius and the porous layer thickness when the Rayleigh number is low ($\mathrm{Ra} = 10^3$)

When the effect of the number of undulation is negligible ($N = 0$)

Figure 3 displays streamlines (left) and isotherms (right) for various inner cylinder radius and the porous layer thickness when ($\mathrm{Ra} = 10^3$, $\mathrm{Da} = 5 \times 10^{-5}$, $\Omega = 3000$, $N = 0$ and $\phi = 0.02$). The flow field inside the trapezoidal enclosure was produced due to the temperature difference between the hot bottom wall and the cold upper

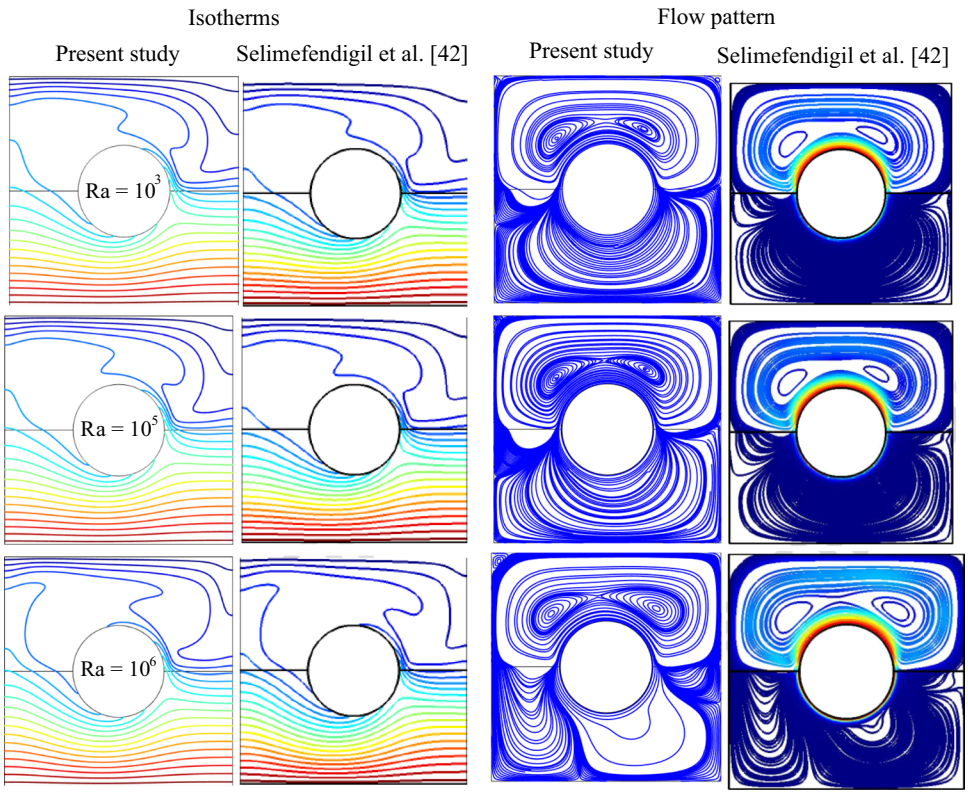

Fig. 2 Comparison of the thermal and the fluid patterns for different Rayleigh numbers with Selimefendigil et al. [42] at ($R=0.2$, $\Omega=3000$, $\phi = 0.02$)

Table 3 Comparison of the average Nusselt number along the hot wall for different Rayleigh numbers ($\Omega=3000$, $\varphi=0.02$, $\mathrm{Da}=5\times10^{-5}$ and $R=0.2$)

Ra	Average Nusselt number at the hot bottom wall		Error/%
	Present study	Selimefendigil et al. [42]	
103	1.93	1.9	− 1.57
104	1.94	1.91	− 1.570
105	1.95	1.915	− 1.827
106	2.01	1.99	− 1.005

one. Therefore, the flow vortices start from the bottom wall due to its high temperature and move by the buoyancy force effect to the adjacent insulated left sidewall. After that, they change their direction to the insulated right sidewall after impacting with the cold upper wall. This cyclic movement leads to produce the convection vortices inside the enclosure. It is very useful to mention that the mixed convection in the enclosure is due to the two effects. The first one is due to the shear force which comes from the rotation of the insulated circular cylinder, while the second effect is due to the buoyancy force as mentioned above. It can be noticed from the flow field pattern that as the porous layer thickness increases, the stream function values begin to decrease. This behavior is observed for all considered range of the inner cylinder radius. For example, when the inner cylinder is small (i.e., $R=0.1$), the stream function decreases from ($\Psi_{\max}=33.617$) when ($S=0.2$) to ($\Psi_{\max}=3.200$) when ($S=0.8$). The same behavior can be observed for medium and large cylinders. Therefore, it can be concluded that as the porous layer thickness inside the enclosure increases, it leads to reduce the rapid increasing in the strength of the flow circulation and to decrease also in the effect of increasing the inner cylinder radius. With respect to the effect of the inner cylinder radius on the flow field, it can seen from the results that as the inner cylinder radius increases from ($R=0.1$) to ($R=0.3$), the stream function values increase. This behavior can be seen for medium and large thickness of the porous layer (i.e., $0.5\le S\le0.8$). For example, when the porous layer thickness is medium (i.e., $S=0.5$), the stream function increases from ($\Psi_{\max}=3.4531$) when ($R=0.1$) to ($\Psi_{\max}=11.662$) when ($R=0.3$). This means that the strength of the flow circulation is high when the cylinder radius is high and vice versa. The reason for this behavior is due to the high reduction of the free space or gap between the enclosure walls and the rotating cylinder surface when its radius is high. This makes the convection currents move much faster between the hot bottom and the cold top walls and leads to increase in the stream function values. With respect to the flow field pattern, it can be

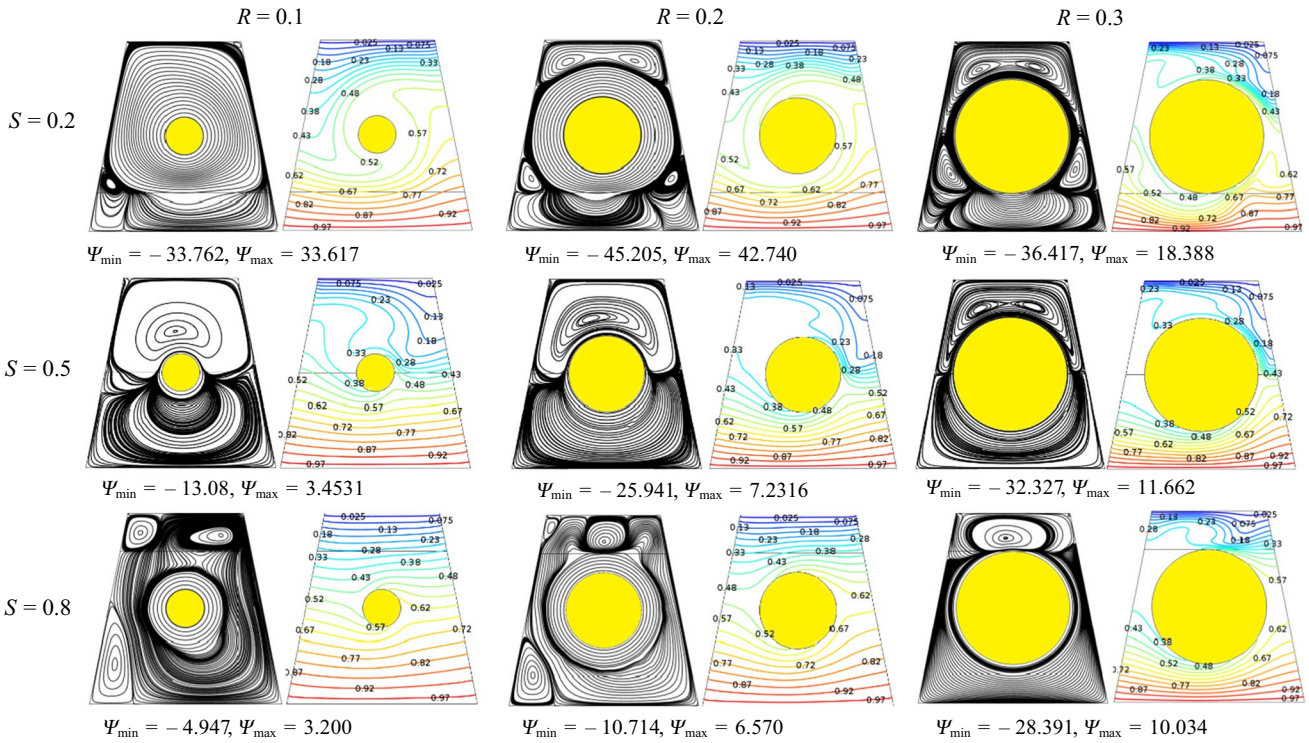

Fig. 3 Streamlines (left) and isotherms (right) for different inner cylinder radius and porous layer thickness at $\mathrm{Ra}=10^3$, $\mathrm{Da}=5\times10^{-5}$, $\Omega=3000$, $N=0$ and $\varphi=0.02$

observed that it consists of two major vortices around the inner cylinder and their size of course decreases as the cylinder radius increases. But, when the thickness of the porous layer is small ($S=0.2$), it can be noticed that as the inner cylinder radius increases from ($R=0.1$) to ($R=0.2$), the stream function increases from ($\Psi_{\max}=33.617$) to ($\Psi_{\max}=42.740$) and then decreases to ($\Psi_{\max}=18.388$) at ($R=0.3$). Furthermore, the flow field pattern consists of multi-cellular vortices which cover all the domain of the enclosure. With respect to the thermal field, it can be seen from isotherm contours that the convection effect is dominant for low and middle values of the porous layer thickness (i.e., $S=0.2$ and 0.5). This behavior can be confirmed from the confused and non-uniform pattern of isotherms especially in the core of the enclosure and around the inner cylinder. This observation is noticed for all considered values of (R). But, as the porous layer thickness increases to ($S=0.8$), the isotherm contours begin to change its behavior to be much uniform and linear shape style than that the corresponding isotherms which are noticed at ($S=0.2$ and 0.5). This indicated that the increase in the porous layer thickness inside the enclosure weakens the heat transfer by the convection and makes the heat conduction inside the enclosure more dominant. Again, this notation is seen for all values of (R). From the another side, similar observation for both the flow and thermals fields can be noticed at ($\mathrm{Ra}=10^5$) as presented in Fig. 4.

When the effect of the number of undulation is considered ($N=1$)

Figures 5 and 6 illustrate, respectively, streamlines (left) and isotherms (right) for various inner cylinder radius and the porous layer thickness at ($\mathrm{Da}=5\times10^{-5}$, $\Omega=3000$, $N=1$ and $\varphi=0.02$) for ($\mathrm{Ra}=10^3$ and 10^5). It can seen that the stream function values begin to decrease when the bottom wall of the enclosure is considered wavy (i.e., $N=1$) compared with their corresponding values when it considered flat as shown previously in Figs. 3 and 4. This difference is large for smaller cylinder and the porous layer thickness (i.e., $R=0.1$ and $S=0.2$) and begins to decrease as both of them increase. Therefore, it can be concluded that the existence of undulations in the bottom wall leads to decrease in the intensity of the flow circulation compared with the flat one. The reason behind this behavior is due to the narrow space between the hot wavy wall and the cylinder surface which leads to restrict the rise-up of the hot fluid and makes the flow circulation more slow. It is useful to mention that this

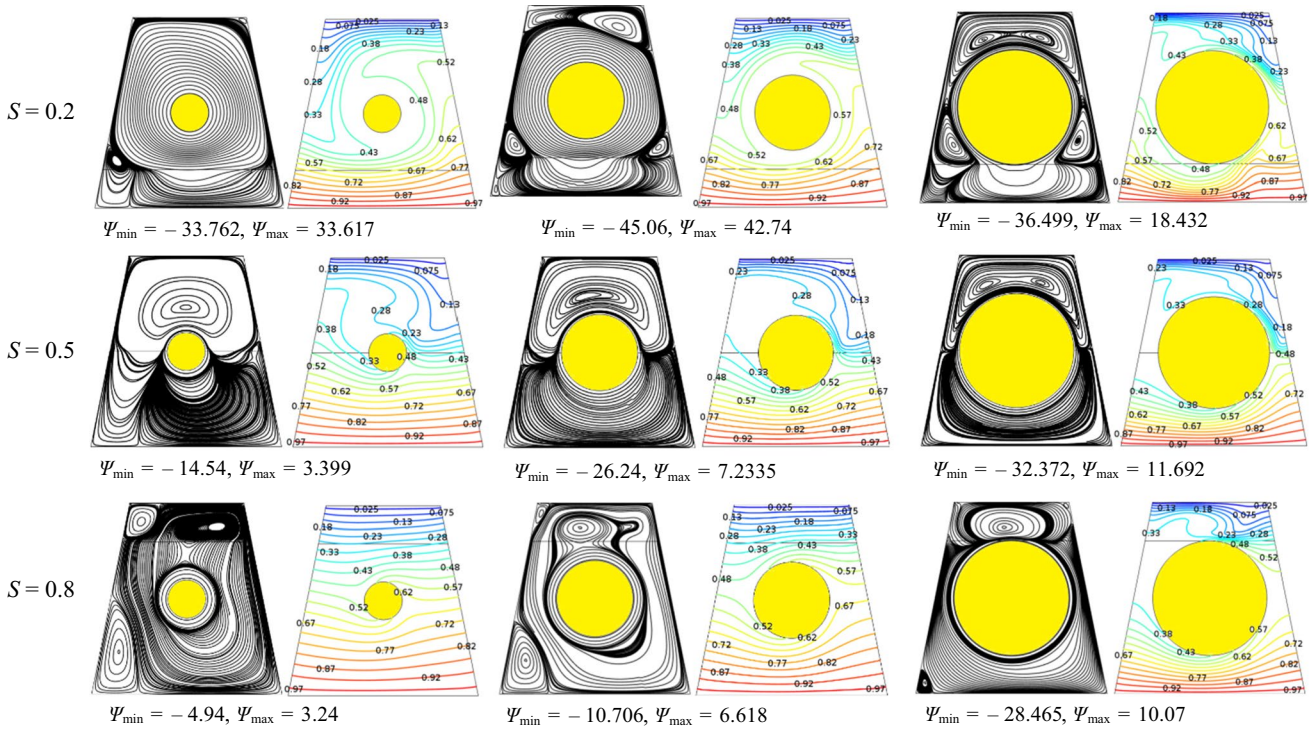

Fig. 4 Streamlines (left) and isotherms (right) for different inner cylinder radius and porous layer thickness at $Ra = 10^5$, $Da = 5 \times 10^{-5}$, $\Omega = 3000$, $N = 0$ and $\varphi = 0.02$

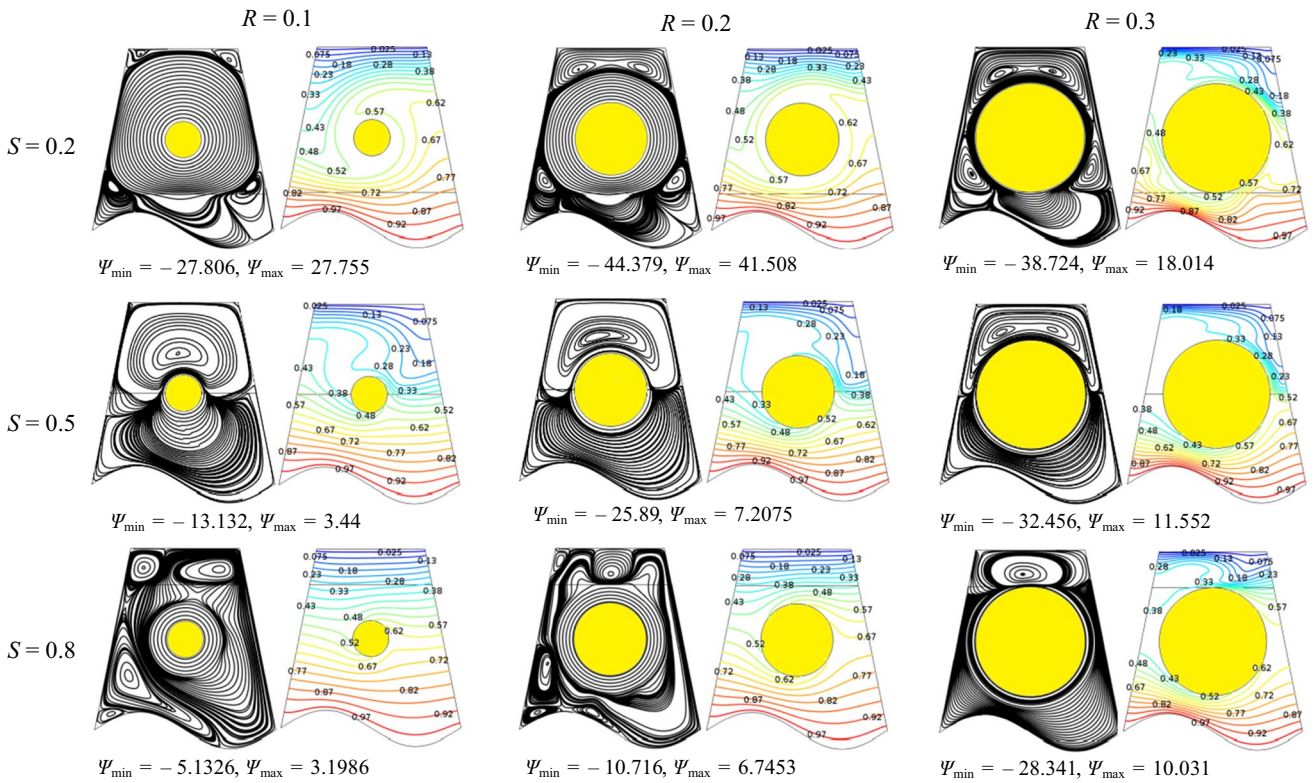

Fig. 5 Streamlines (left) and isotherms (right) for different inner cylinder radius and porous layer thickness at $Ra = 10^3$, $Da = 5 \times 10^{-5}$, $\Omega = 3000$, $N = 1$ and $\varphi = 0.02$

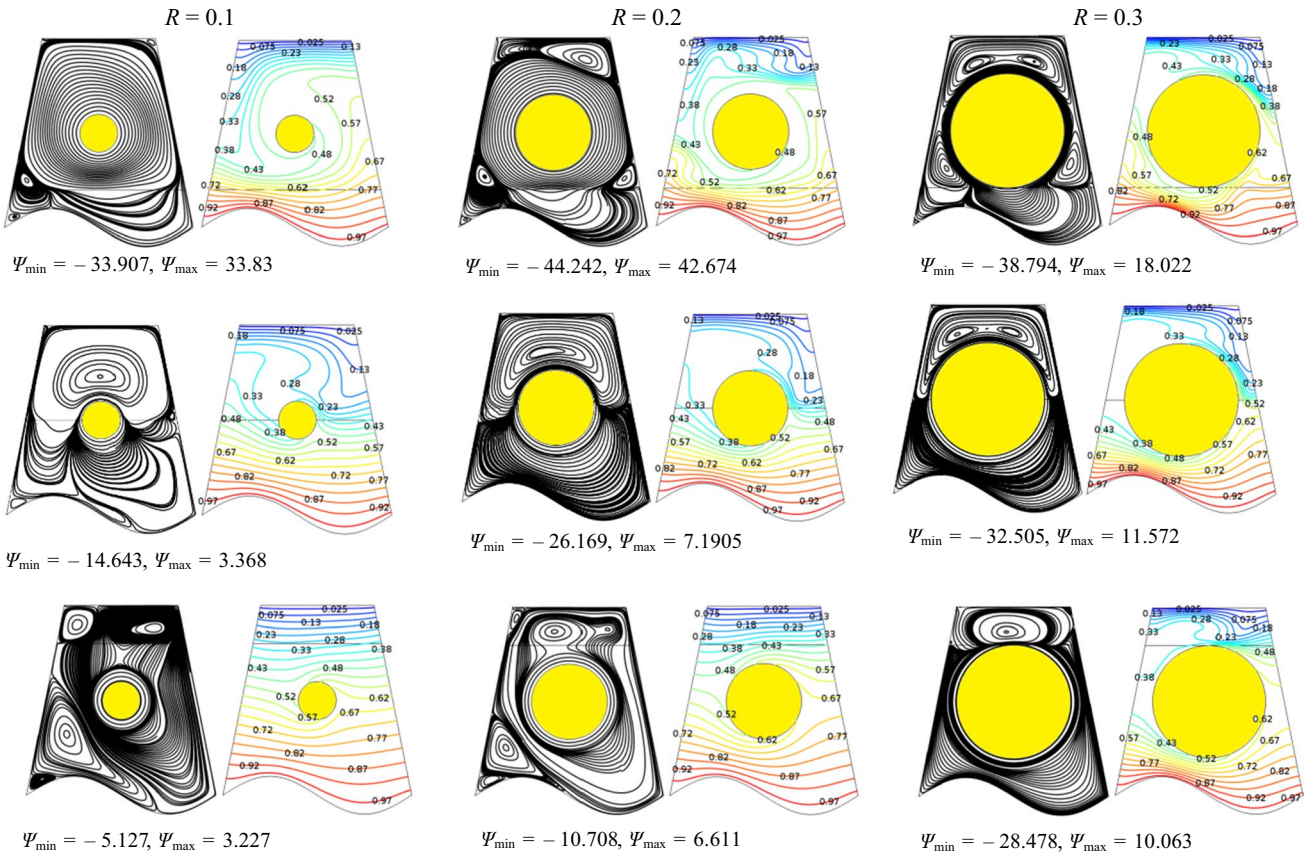

Fig. 6 Streamlines (left) and isotherms (right) for different inner cylinder radius and porous layer thickness at $\mathrm{Ra}=10^5$, $\mathrm{Da}=5\times10^{-5}$, $\Omega=3000$, $N=1$ and $\varphi=0.02$

effect is more severe for ($S=0.2$) and decreases gradually as the porous layer thickness increases. The same notation can be seen for ($\mathrm{Ra}=10^5$) except for ($R=0.1$ and $S=0.2$) case. On the other hand, it can be observed from the flow field pattern that the stream function values decrease as the porous layer thickness increases. With respect to the inner cylinder radius effect, it can be noticed that for ($S=0.2$), the stream function increases as the inner cylinder radius increases and then decreases at ($R=0.3$), while for ($S=0.5$ and 0.8), it increases as the inner cylinder radius increases. Furthermore, the existence of the undulation in the bottom wall leads to trap the flow circulation in the wavy wall and reduces the effect of the convection. Moreover, the isotherm patterns are affected also by the undulated wall. They converge at the crests of the wavy wall and diverge at the troughs of it, so it plays also as an additional factor to make the conduction more dominant especially in the lower half of the enclosure.

Effect of the Darcy number on the flow and thermal fields

The streamlines (top) and isotherms (bottom) for various Darcy and Rayleigh numbers at ($\Omega=3000$, $\varphi=0.02$, $R=0.2$, $N=1$ and $S=0.5$) are presented in Fig. 7 for the trapezoidal enclosure with a wavy bottom wall. It can be seen that for both considered values of the Rayleigh number (i.e., $\mathrm{Ra}=10^3$ and 10^5), the stream function decreases as the Darcy number decreases from ($\mathrm{Da}=10^{-2}$) to ($\mathrm{Da}=10^{-5}$). So, it decreases at ($\mathrm{Ra}=10^3$) from ($\Psi_{max}=53.58$) when ($\mathrm{Da}=10^{-2}$) to ($\Psi_{max}=3.15$) when ($\mathrm{Da}=10^{-5}$). The same behavior can be observed at ($\mathrm{Ra}=10^5$). Therefore, it can be seen that when the Darcy number is high ($\mathrm{Da}=10^{-2}$), the strength of the flow circulation is high also and the flow field can be represented by a major rotating vortex which lies near the inner cylinder and covers all the size of the enclosure. Moreover, minor vortices can be observed also at the edges of the straight cold top wall and the wavy hot bottom one. In fact, for high Darcy number (i.e., $\mathrm{Da}=10^{-2}$), the viscous effect on the flow circulation related with the porous

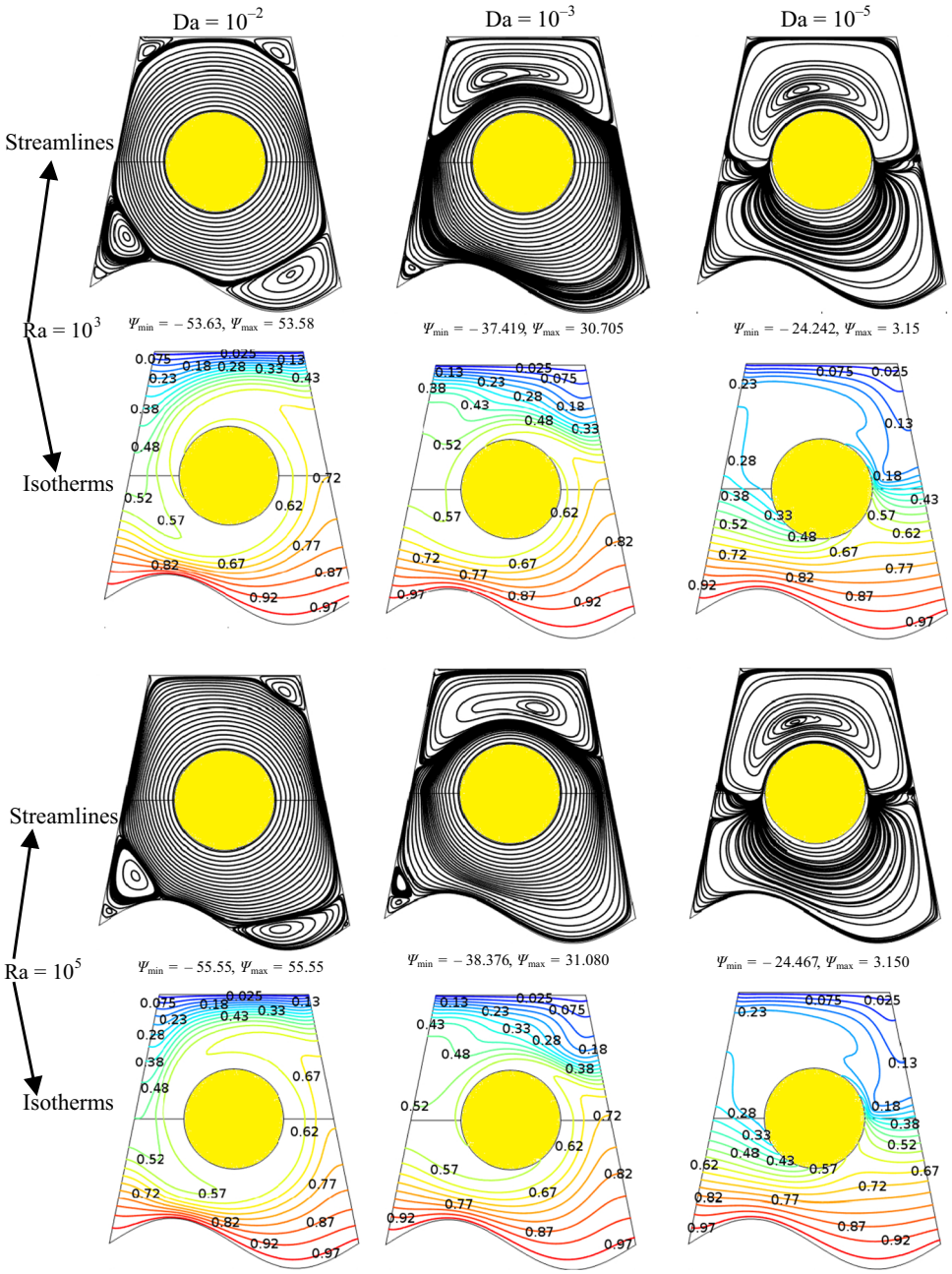

Fig. 7 Streamlines (top) and isotherms (bottom) for various Darcy and Rayleigh numbers at ($\Omega = 3000$, $\varphi = 0.02$, $R = 0.2$, $N = 1$ and $S = 0.5$)

media term is significant. Therefore, the permeability of the porous media is also high, since the permeability of the porous media is directly proportional to the Darcy number. Therefore, for these reasons the strength of the flow circulation is high when the Darcy number is high as shown in Fig. 7. Now, as the Darcy number decreases to ($\mathrm{Da} = 10^{-5}$), a severe reduction in the stream function values can be noticed. So, it can be concluded that the flow circulation becomes weak for small values of the Darcy number. Also, a clear change in the flow field pattern can be noted, since it consists of two rotating vortices around the inner cylinder, while the minor vortices which are noticed previously disappear completely. The maximum value of the stream function can be observed at high values of the Darcy and the Rayleigh numbers (i.e., $\mathrm{Ra} = 10^5$ and $\mathrm{Da} = 10^{-2}$). With respect to the thermal field, it can be seen from the isotherm contours that when the Darcy number is high ($\mathrm{Da} = 10^{-2}$), a clear confusion in their pattern is seen. They are started from the hot bottom wall and move inside the enclosure until they reach to the cold top wall. From the opposite side, as the Darcy number decreases, the reduction in the flow circulation makes the

isotherms symmetrical and parallel to each other especially in the porous media region, while the conduction becomes dominant. Again, similar observations can be seen at ($Ra = 10^5$).

Effect of the solid volume fraction on the flow and thermal fields

Figure 8 illustrates streamlines (top) and isotherms (bottom) for various Rayleigh numbers and solid volume fraction (red line for the nanofluid with ($\varphi = 0.06$) and green line for the water ($\varphi = 0$)) and ($Da = 5 \times 10^{-5}$, $\Omega = 3000$, $R = 0.2$, $N = 2$ and $S = 0.5$). It can be noticed from the flow field pattern that there is a slight variation in the stream function values between the base fluid (i.e., water) and the nanofluid (i.e., CuO–water). Moreover, a similar flow field pattern which consists of two rotating unsymmetrical vortices around the inner cylinder can be seen for both base and nanofluids. This behavior can be observed for both considered values of the Rayleigh number (i.e., $Ra = 10^3$ and 10^5). Therefore, it can be deduced that for both considered values of the Rayleigh number ($Ra = 10^3$ and 10^5), a slight variation in the flow field pattern can be observed by increasing the solid volume fraction especially in the pure nanofluid region. With respect to the isotherm contours, it can be noticed again from the results in Fig. 8 that the increasing of the solid volume fraction does not alter their pattern significantly. This behavior can be seen for both top and bottom regions of the enclosure.

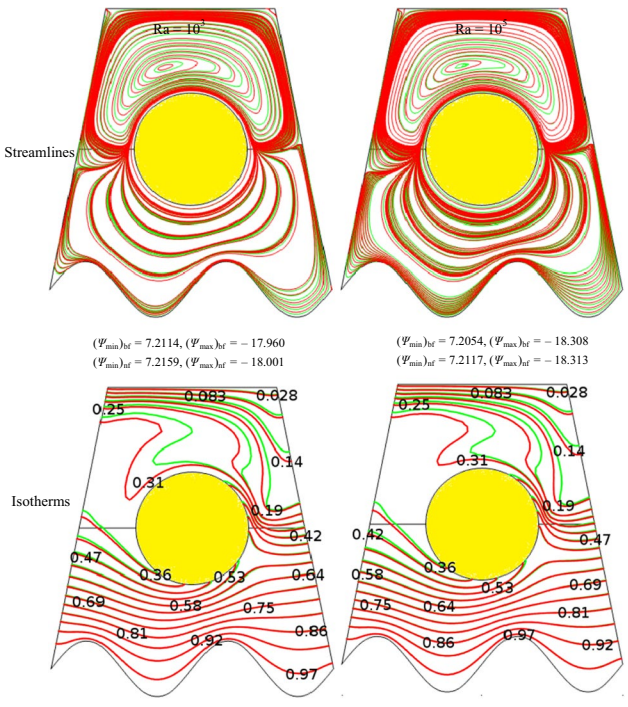

Fig. 8 Streamlines (top) and isotherms (bottom) for various Rayleigh numbers and solid volume fraction (red line, $\varphi = 0.06$ and green line, $\varphi = 0$) and $Da = 5 \times 10^{-5}$, $\Omega = 3000$, $R = 0.2$, $N = 2$ and $S = 0.5$

Effect of the angular rotational velocity on the flow and thermal fields

The streamlines (top) and isotherms (bottom) for various Rayleigh numbers and angular rotational velocity of the cylinder at ($Da = 5 \times 10^{-5}$, $\varphi = 0.02$, $R = 0.2$, $N = 3$ and $S = 0.5$) are displayed in Fig. 9 for the trapezoidal enclosure with a wavy bottom wall. The results referred that the stream function increases as the angular rotational velocity increases, and this behavior is seen when the Rayleigh number is low (i.e., $Ra = 10^3$).This increasing is due to the high interaction which occurs between the cylinder surface and the hot fluid which comes from the bottom wall. This leads to make more flow crosses toward the upper cold region of the enclosure and increases the stream function values. For example at ($Ra = 10^3$), when the inner cylinder is considered stationary (i.e., $\Omega = 0$), the stream function is very low ($\Psi_{max} = 0.00538$) and it increases gradually with the increase in the angular rotational velocity of the cylinder until it reaches ($\Psi_{max} = 14.525$) at ($\Omega = 6000$). When the Rayleigh number becomes high (i.e., $Ra = 10^6$), it can be seen that the stream function value is high, when the inner cylinder is considered stationary (i.e., $\Omega = 0$). But, as the cylinder begins to move, the stream function decreases from ($\Psi_{max} = 8.181$) at ($\Omega = 0$) to ($\Psi_{max} = 4.85$) at ($\Omega = 2000$). This decreasing is due to the opposite directions of rotation between the cylinder and the flow that leads to a decrease of the stream function value. After that, as the angular rotational velocity increases gradually, the stream function values begin to increase secondly. With respect to the effect of the angular rotational velocity of the cylinder on the flow field pattern, it can be seen from the results which are illustrated in Fig. 9 that there is a clear change occured in it. The flow pattern switches their shape from a multi-cellular vortices which are noticed around the cylinder at ($\Omega = 0$) into a two unsymmetrical major rotating vortices when the cylinder is considered to rotate ($2000 \leq \Omega \leq 6000$). Also, it can be noticed that vortices in the nanofluid region (upper half of the enclosure) are more intense than the corresponding vortices in the porous region (lower half of the enclosure) especially for the rotating cylinder case. This behavior can be returned to the existence of the porous layer which leads to decrease in the effect of the cylinder rotation and makes the vortices less intense. The another point which is necessary to clarify it is that the multi-cellular vortices which are noticed in the porous region disappear when the cylinder is considered fixed, while they diminish completely in the same region by the rotation of the inner cylinder as mentioned above. Also, it can be seen that the vortices begin to confuse and clustered strongly by increasing the Rayleigh number especially in the porous region. This is of course due to the high effect of the convection by increasing the Rayleigh number. With respect

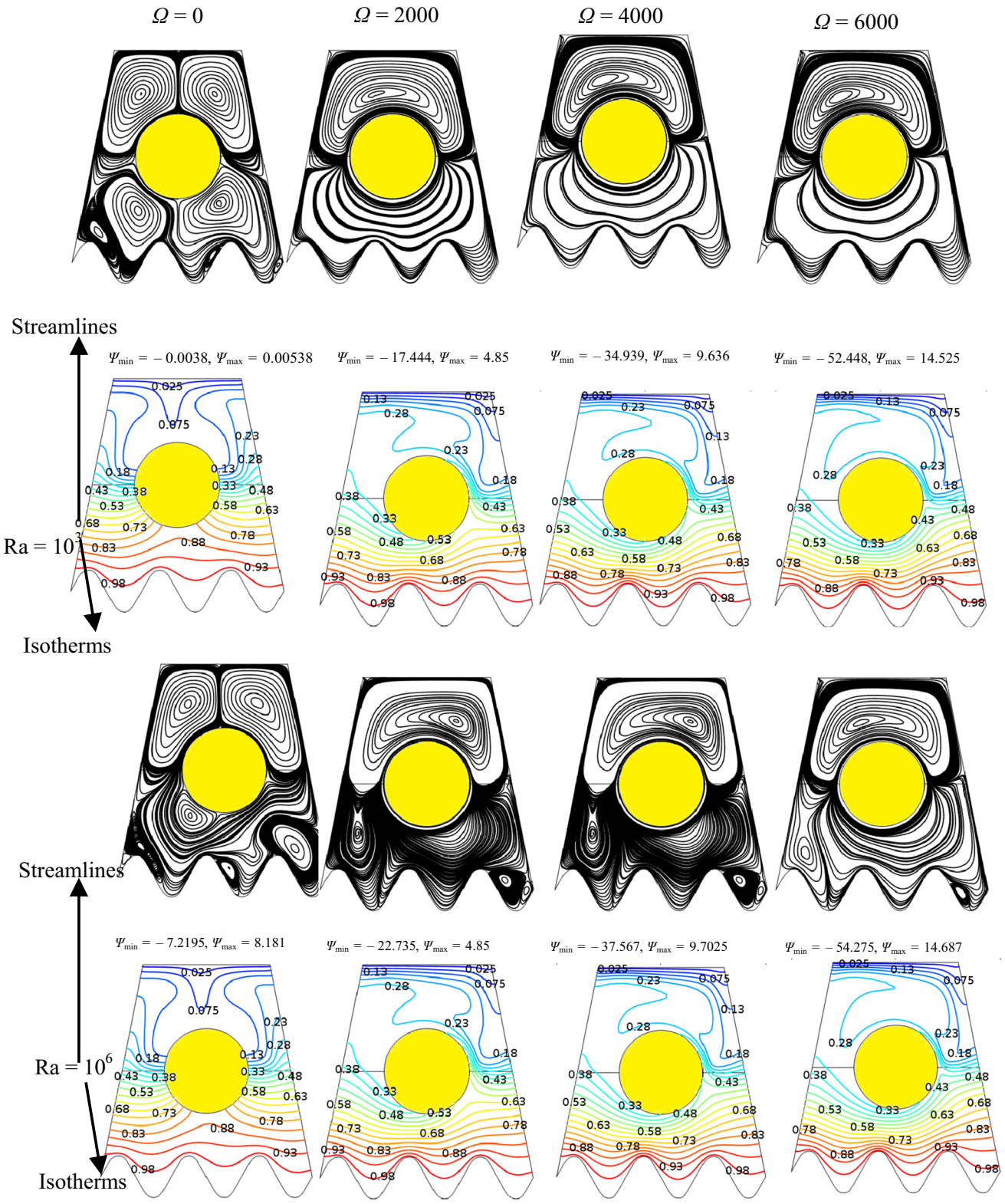

Fig. 9 Streamlines (top) and isotherms (bottom) for various Rayleigh numbers and angular rotational velocity of the cylinder at $\mathrm{Da}=5\times10^{-5}$, $\varphi=0.02$, $R=0.2$, $N=3$ and $S=0.5$)

to the thermal field, it can be seen from the isotherms pattern that when the cylinder is considered stationary, the heat is transferred inside the enclosure by the conduction. This conclusion is based on the uniform structure of isotherms at ($\Omega = 0$). But, when it considered to rotate ($2000 \le \Omega \le 6000$), the isotherms begin to confuse clearly especially in the nanofluid region. This refers that the convection becomes more effective in this case.

Average Nusselt number results

Figure 10 displays the variation in the average Nusselt number along the hot wavy wall for various Rayleigh numbers and solid volume fraction at ($\mathrm{Da} = 5 \times 10^{-5}$, $\Omega = 3000$, $S = 0.5$, $N = 1$ and $R = 0.2$). As illustrated in this figure, the average Nusselt number increases as the Rayleigh number and the solid volume fraction increase. The reason for this behavior is due to the enhancement in the convection heat transfer inside the enclosure with increasing the Rayleigh number, and this leads to increase in the average Nusselt number results. Also, the same result can be found by increasing the solid volume fraction. This is due to the high enhancement in the thermal conductivity of the base fluid by adding a nanoparticles, and this leads to improve the heat transfer rate inside the enclosure and increases the average Nusselt number. Therefore, it can be concluded that the highest values of the average Nusselt number correspond to the highest values of (Ra) and (φ). Also, it can deduced from the results that the using of CuO–water nanofluid leads to enhance the heat transfer process compared with the pure water ($\varphi = 0$) especially for high values of the solid volume fraction (i.e., $\varphi = 0.06$) as mentioned previously. Figure 11 displays the variation in the average Nusselt number along the hot wall for various Rayleigh and Darcy numbers at ($\Omega = 3000$, $\varphi = 0.02$, $S = 0.5$, $N = 0$ and $R = 0.2$). Again, it

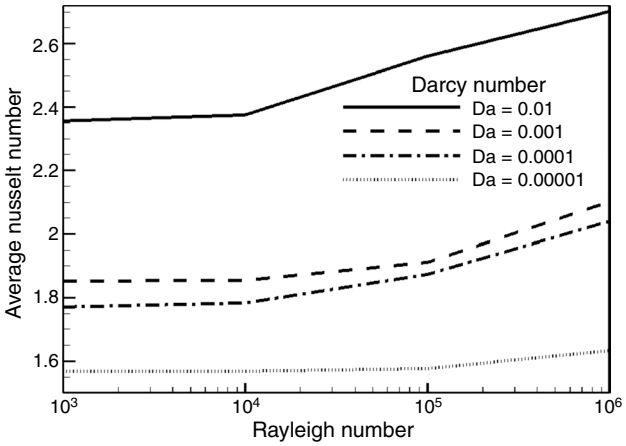

Fig. 11 The variation in the average Nusselt number along the hot wall for various Rayleigh and Darcy numbers at $\Omega = 3000$, $\varphi = 0.02$, $S = 0.5$, $N = 0$, $R = 0.2$

can be found that the average Nusselt number increases as the Darcy number increases. Therefore, it can be concluded that the heat exchange process is better for the highest value of the Darcy number (i.e., $\mathrm{Da} = 10^{-2}$). This is a logical result due to the positive effect of the convection when the Darcy number is high. The reason for this behavior is due to the increase in the permeability of the porous media by increasing the Darcy number. This leads to decrease in the resistance of the porous layer against the flow circulation and enhances the activity of the convection inside the enclosure which leads as a result to increase in the average Nusselt number values. Figure 12 depicts the variation in the average Nusselt number along the hot wavy wall for various Rayleigh

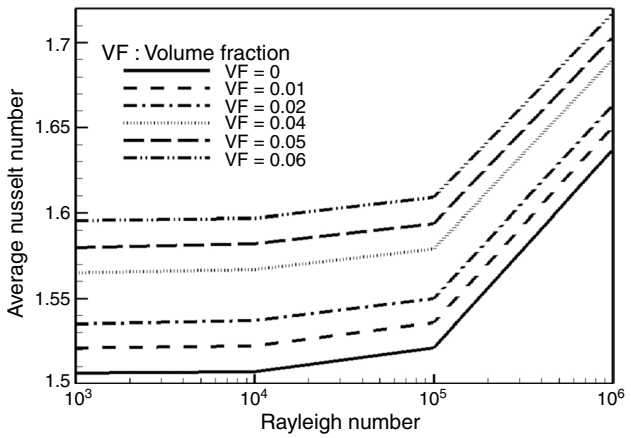

Fig. 10 The variation in the average Nusselt number along the hot wall for various Rayleigh numbers and solid volume fraction at ($\mathrm{Da} = 5 \times 10^{-5}$, $\Omega = 3000$, $S = 0.5$, $N = 1$, $R = 0.2$)

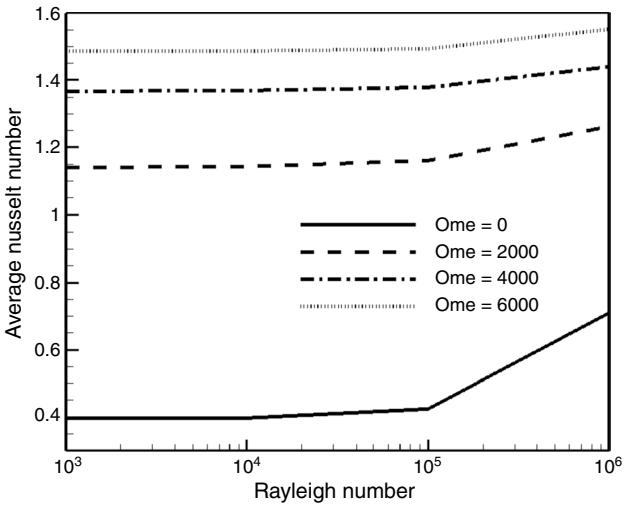

Fig. 12 The variation in the average Nusselt number along the hot wall for various Rayleigh numbers and angular rotational velocity of the cylinder at $\mathrm{Da} = 5 \times 10^{-5}$, $\varphi = 0.02$, $S = 0.5$, $N = 2$, $R = 0.2$)

numbers and the angular rotational velocity of the cylinder at ($Da = 5 \times 10^{-5}$, $\varphi = 0.02$, $S = 0.5$, $N = 2$ and $R = 0.2$). It can be observed that the average Nusselt number increases as the angular rotational velocity of the cylinder increases. This is of course due to the increase in the shear force effect by increasing the angular rotational velocity. This causes an improvement in the mixed convection role inside the enclosure and leads to a significant improvement in the average Nusselt number. Therefore, it can be seen from Fig. 12 that the maximum average Nusselt number occurs for the highest angular rotational velocity of the cylinder (i.e., $\Omega = 6000$).

The variation in the average Nusselt number with the Rayleigh number along the hot wall for different porous layer thickness, radius of inner rotating cylinder and number of undulations at ($\Omega = 3000$, $\varphi = 0.2$ and $Da = 10^{-5}$) is illustrated in Fig. 13. It can be seen from this figure that the average Nusselt number decreases as the porous layer thickness increases from ($S = 0.2$) to ($S = 0.8$). It is to be noted that the resistance of the porous layer against the flow circulation increases as its thickness increases. This weakens the influence of the convection and decreases the average Nusselt number. From the another side, it can be seen that

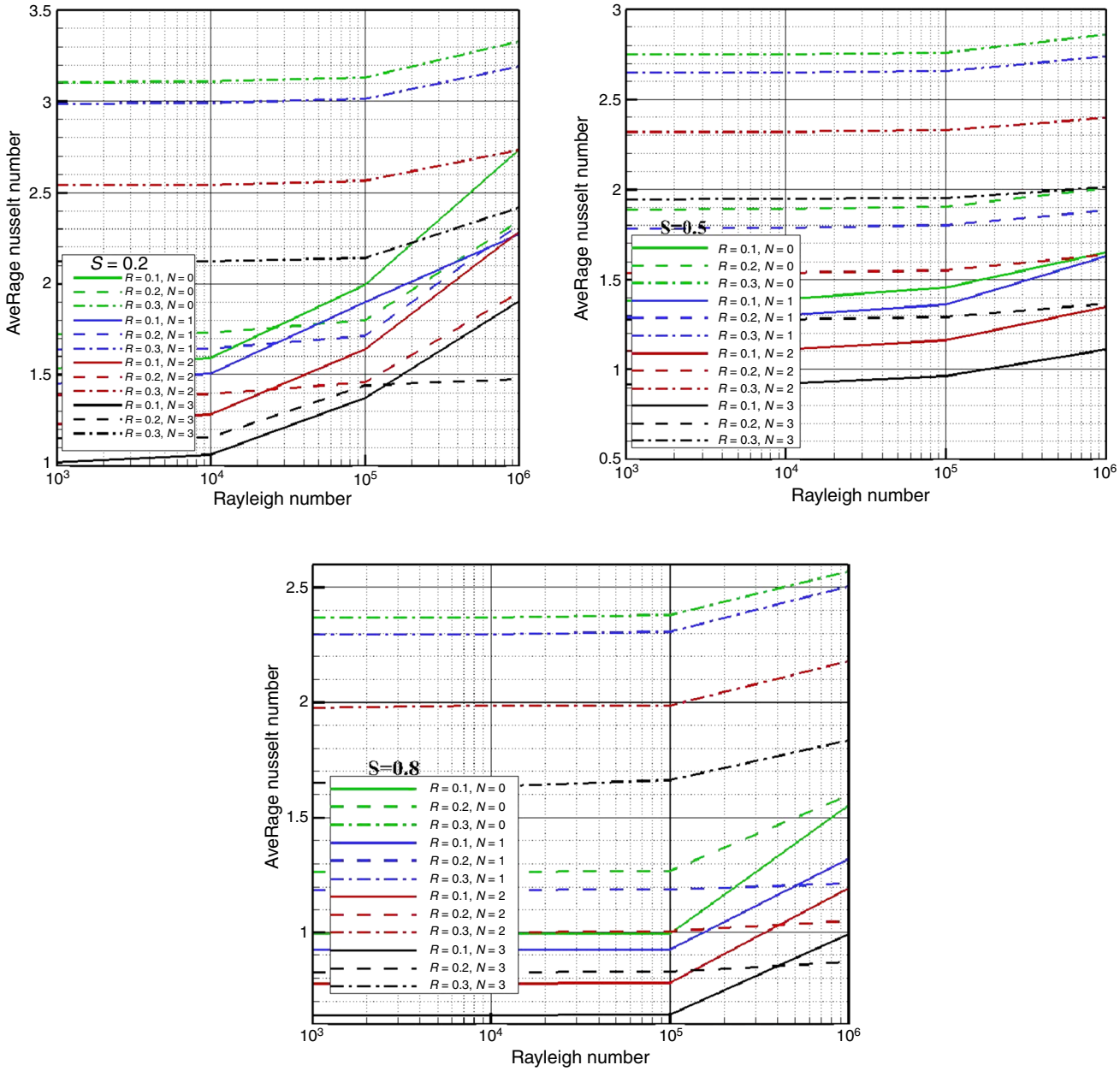

Fig. 13 The variation in the average Nusselt number with the Rayleigh number along the hot wall for different porous layer thickness, radius of rotating cylinder and number of undulations at $\Omega = 3000$, $\varphi = 0.2$ and $Da = 10^{-5}$

the average Nusselt number increases as the inner cylinder radius increases. Since, the flow circulation is much higher for a larger cylinder radius increases and the flow circulation is more intense for larger cylinder diameter. The reason for this enhancement can be returned to the reduction in the gap between the enclosure horizontal walls and the cylinder surface which makes the convection heat transfer more faster and enhances the average Nusselt number. With respect to the effect of the number of undulations on the average Nusselt number results, it can be seen that they decrease as the number of undulations increases. The reason behind this behavior is due to the drag effect caused by the protruding segments of the wavy bottom wall which leads to decrease in the average Nusselt number. Therefore, it can be concluded that the average Nusselt number reaches it maximum value when the bottom wall of the enclosure is considered flat (i.e., $N=0$).

Conclusions

The laminar mixed convection in a trapezoidal enclosure with a rotating inner circular cylinder and a sinusoidal bottom wall is studied numerically. The fluid inside the enclosure is a CuO–water nanofluid layer in the top space of it, while the bottom space includes a CuO–water nanofluid saturated with a porous medium. It was found that for ($\mathrm{Ra}=10^3$ and $N=0$), as the porous layer thickness increases, the stream function values begin to decrease sharply for ($0.1\le R\le 0.2$) and slightly for ($R=0.3$). For ($\mathrm{Ra}=10^3$ and $N=0$) and ($0.5\le S\le 0.8$), it can be seen that as the inner cylinder radius increases from ($R=0.1$) to ($R=0.3$), the stream function values increase continuously. But, for ($S=0.2$), a different behavior is noticed. Also, it can be noticed that for ($\mathrm{Ra}=10^3$ and $N=0$), when the porous layer thickness inside the enclosure increases, it leads to reduce the rapid increasing in the strength of the flow circulation and to decrease also in the effect of increasing the inner cylinder radius.

For ($\mathrm{Ra}=10^3$ and $N=0$) and all considered values of (R), the isotherm lines in the porous layer region are much linear and uniform than the corresponding isotherms in the pure nanofluid region. Also, they become much slim for high values of the porous layer thickness (i.e., $S=0.8$). This gives a clear indication that for high values of (S), the conduction mode of the heat transfer is dominant. From the another side, for both ($\mathrm{Ra}=10^3$ and 10^5), a slight variation in the flow and thermal fields can be observed by increasing the solid volume fraction for the wavy enclosure especially in the pure nanofluid region. The strength of the convection inside the wavy enclosure increases as the Darcy number increases. In addition, the isotherms become more distorted and the convection is dominant when the Darcy number is high. The effect of the increasing of the angular rotational velocity of the cylinder in the porous layer region is small than its effect in the nanofluid region. Also, the convection is dominant by increasing the angular rotational velocity. The existence of undulations in the bottom wall leads to decrease in the intensity of the flow circulation and makes the conduction effect more dominant. The average Nusselt number increases as the Rayleigh and Darcy numbers, the solid volume fraction, inner cylinder radius and the angular rotational velocity of the cylinder increase, while it decreases as the porous layer thickness and the number of undulations increase. In order to add some future directions and outlook of the present work, one can study the entropy generation or consider the three-dimensional investigation for the same geometry.

Acknowledgements The fourth author would like to acknowledge the research deanship of University of Ha'il, KSA for funding the project "191225".

References

1. Choi U. Enhancing thermal conductivity of fluids with nanoparticles. In: Siginer DA, Wang HP, (editors). Developments and applications of non-Newtonian flows, FED 231, 1995, pp. 99–105.
2. Chand R, Rana G, Hussein AK. On the onset of thermal instability in a low Prandtl number nanofluid layer in a porous medium. J Appl Fluid Mech. 2015;8(2):265–72.
3. Chand R, Rana G, Hussein AK. Effect of suspended particles on the onset of thermal convection in a nanofluid layer for more realistic boundary conditions. Int J Fluid Mech Res. 2015;42(5):375–90.
4. Hussein AK, Walunj A, Kolsi L. Applications of nanotechnology to enhance the performance of the direct absorption solar collectors. J Therm Eng. 2016;2(1):529–40.
5. Hussein AK. Applications of nanotechnology in renewable energies-A comprehensive overview and understanding. Renew Sustain Energy Rev. 2015;42:460–76.
6. Hussein AK. Applications of nanotechnology to improve the performance of solar collectors—recent advances and overview. Renew Sustain Energy Rev. 2016;62:767–92.
7. Hussein AK, Li D, Kolsi L, Kata S, Sahoo B. A review of nano fluid role to improve the performance of the heat pipe solar collectors. Energy Proc. 2017;109:417–24.
8. Mahian O, Kolsi L, Amani M, Estellé P, Ahmadi G, Kleinstreuer C, Marshall J, Siavashi M, Taylor R, Niazmand H, Wongwises S, Hayat T, Kolanjiyil A, Kasaeian A, Pop I. Recent advances in modeling and simulation of nanofluid flows—part I: fundamentals and theory. Phys Rep. 2019;790:1–48.
9. Mahian O, Kolsi L, Amani M, Estellé P, Ahmadi G, Kleinstreuer C, Marshall J, Taylor R, Abu-Nada E, Rashidi S, Niazmand H, Wongwises S, Hayat T, Kasaeian A, Pop I. Recent advances in modeling and simulation of nanofluid flows—part II: applications. Phys Rep. 2019;791:1–59.
10. Sivasankaran S, Sivakumar V, Hussein AK. Numerical study on mixed convection in an inclined lid-driven cavity with discrete heating. Int Commun Heat Mass Transf. 2013;46:112–25.
11. Sivasankaran S, Sivakumar V, Hussein AK, Prakash P. Mixed convection in a lid-driven two-dimensional square cavity with corner heating and internal heat generation. Numer Heat Transf Part A. 2014;65:269–86.

12. Ismael M, Ghalib H. Double diffusive natural convection in a partially layered cavity with inner solid conductive body. Sci Iranica B. 2018;25(5):2643–59.
13. Bhuvaneswari M, Eswaramoorthi S, Sivasankaran S, Hussein AK. Cross-diffusion effects on MHD mixed convection over a stretching surface in a porous medium with chemical reaction and convective condition. Eng Trans. 2019;67(1):3–19.
14. Hussein AK, Hussain S. Mixed convection through a lid-driven air-filled square cavity with a hot wavy wall. Int J Mech Mater Eng (IJMME). 2010;5(2):222–35.
15. Saha S, Hussein AK, Saha G, Hussain S. Mixed convection in a tilted lid-driven square enclosure with adiabatic cylinder at the center. Int J Heat Technol. 2011;29(1):143–56.
16. Gangawane K, Oztop H, Abu-Hamdeh N. Mixed convection characteristic in a lid-driven cavity containing heated triangular block: effect of location and size of block. Int J Heat Mass Transf. 2018;124:860–75.
17. Chakravarty A, Datta P, Ghosh K, Sen S, Mukhopadhyay A. Mixed convective heat transfer in an enclosure containing a heat generating porous bed under the influence of bottom injection. Int J Heat Mass Transf. 2018;117:645–57.
18. Taghizadeh S, Asaditaheri A. Heat transfer and entropy generation of laminar mixed convection in an inclined lid driven enclosure with a circular porous cylinder. Int J Therm Sci. 2018;134:242–57.
19. Alsabery A, Tayebi T, Chamkha A, Hashim I. Effect of rotating solid cylinder on entropy generation and convective heat transfer in a wavy porous cavity heated from below. Int Commun Heat Mass Transf. 2018;95:197–209.
20. Mahalakshmi T, Nithyadevi N, Oztop H, Abu-Hamdeh N. MHD mixed convective heat transfer in a lid-driven enclosure filled with Ag-water nanofluid with center heater. Int J Mech Sci. 2018;142–143:407–19.
21. Yu Q, Xu H, Liao S. Analysis of mixed convection flow in an inclined lid-driven enclosure with Buongiorno's nanofluid model. Int J Heat Mass Transf. 2018;126:221–36.
22. Zhou W, Yan Y, Liu X, Chen H, Liu B. Lattice Boltzmann simulation of mixed convection of nanofluid with different heat sources in a double lid-driven cavity. Int Commun Heat Mass Transf. 2018;97:39–46.
23. Mamourian M, Milani Shirvan K, Ellahi R, Rahimi A. Optimization of mixed convection heat transfer with entropy generation in a wavy surface square lid-driven cavity by means of Taguchi approach. Int J Heat Mass Transf. 2016;102:544–54.
24. Cho C. Heat transfer and entropy generation of mixed convection flow in Cu-water nanofluid-filled lid-driven cavity with wavy surface. Int J Heat Mass Transf. 2018;119:163–74.
25. Pal S, Bhattacharyya S, Pop I. Effect of solid-to-fluid conductivity ratio on mixed convection and entropy generation of a nanofluid in a lid-driven enclosure with a thick wavy wall. Int J Heat Mass Transf. 2018;127:885–900.
26. Alsabery A, Ismael M, Chamkha A, Hashim I. Numerical investigation of mixed convection and entropy generation in a wavy-walled cavity filled with nanofluid and involving a rotating cylinder. Entropy. 2018. https://doi.org/10.3390/e20090664.
27. Alsabery A, Sheremet M, Chamkha A, Hashim I. Impact of non-homogeneous nanofluid model on transient mixed convection in a double lid-driven wavy cavity involving solid circular cylinder. Int J Mech Sci. 2019;150:637–55.
28. Alsabery A, Ismael M, Chamkha A, Hashim I. Mixed convection of Al_2O_3–water nanofluid in a double lid-driven square cavity with a solid inner insert using Buongiorno's two-phase model. Int J Heat Mass Transf. 2018;119:939–61.
29. Nayak R, Bhattacharyya S, Pop I. Effects of nanoparticles dispersion on the mixed convection of a nanofluid in a skewed enclosure. Int J Heat Mass Transf. 2018;125:908–19.
30. Garmroodi M, Ahmadpour A, Talati F. MHD mixed convection of nanofluids in the presence of multiple rotating cylinders in different configurations: a two-phase numerical study. Int J Mech Sci. 2019;150:247–64.
31. Hussain S, Mehmood K, Sagheer M. MHD mixed convection and entropy generation of water–alumina nanofluid flow in a double lid driven cavity with discrete heating. J Magn Magn Mater. 2016;419:140–55.
32. Arani A, Ababaei A, Sheikhzadeh G, Aghaei A. Numerical simulation of double-diffusive mixed convection in an enclosure filled with nanofluid using Bejan's heatlines and masslines. Alexandria Eng J. 2018;57:1287–300.
33. Hussain S, Oztop H, Mehmood K, Abu-Hamdeh N. Effects of inclined magnetic field on mixed convection in a nanofluid filled double lid-driven cavity with volumetric heat generation or absorption using finite element method. Chin J Phys. 2018;56:484–501.
34. Sheremet M, Roşca N, Roşca A, Pop I. Mixed convection heat transfer in a square porous cavity filled with a nanofluid with suction/injection effect. Comput Math Appl. 2018;76:2665–77.
35. Gibanov N, Sheremet M, Oztop H, Abu-Hamdeh N. Mixed convection with entropy generation of nanofluid in a lid-driven cavity under the effects of a heat-conducting solid wall and vertical temperature gradient. Eur J Mech B Fluids. 2018;70:148–59.
36. Rajarathinam M, Nithyadevi N, Chamkha A. Heat transfer enhancement of mixed convection in an inclined porous cavity using Cu-water nanofluid. Adv Powder Technol. 2018;29:590–605.
37. Astanina M, Sheremet M, Oztop H, Abu-Hamdeh N. Mixed convection of Al_2O_3–water nanofluid in a lid-driven cavity having two porous layers. Int J Heat Mass Transf. 2018;118:527–37.
38. Xu H, Xing Z, Wang F, Cheng Z. Review on heat conduction, heat convection, thermal radiation and phase change heat transfer of nanofluids in porous media: fundamentals and applications. Chem Eng Sci. 2019;195:462–83.
39. Kareem A, Mohammed H, Hussein AK, Gao S. Numerical investigation of mixed convection heat transfer of nanofluids in a lid-driven trapezoidal cavity. Int Commun Heat Mass Transf. 2016;77:195–205.
40. Chamkha A, Ismael M. Magnetic field effect on mixed convection in lid-driven trapezoidal cavities filled with a Cu-water nanofluid with an aiding or opposing side wall. J Therm Sci Eng Appl. 2016;8:031009-1–-12.
41. Selimefendigil F, Oztop H. Modeling and optimization of MHD mixed convection in a lid-driven trapezoidal cavity filled with alumina-water nanofluid: effects of electrical conductivity models. Int J Mech Sci. 2018;136:264–78.
42. Siavashi M, Bahrami H, Aminian E. Optimization of heat transfer enhancement and pumping power of a heat exchanger tube using nanofluid with gradient and multi-layered porous foams. Appl Therm Eng. 2018;138:465–74.
43. Bozorg M, Siavashi M. Two-phase mixed convection heat transfer and entropy generation analysis of a non-Newtonian nanofluid inside a cavity with internal rotating heater and cooler. Int J Mech Sci. 2019;151:842–57.
44. Asiaei S, Zadehkafi A, Siavashi M. Multi-layered porous foam effects on heat transfer and entropy generation of nanofluid mixed convection inside a two-sided lid-driven enclosure with internal heating. Transp Porous Med. 2019;126(1):223–47.
45. Siavashi M, Rostami A. Two-phase simulation of non-Newtonian nanofluid natural convection in a circular annulus partially or completely filled with porous media. Int J Mech Sci. 2017;133:689–703.
46. Toosi M, Siavashi M. Two-phase mixture numerical simulation of natural convection of nanofluid flow in a cavity partially

filled with porous media to enhance heat transfer. J Mol Liq. 2017;238:553–69.
47. Siavashi M, Yousofvand R, Rezanejad S. Nanofluid and porous fins effect on natural convection and entropy generation of flow inside a cavity. Adv Powder Technol. 2018;29:142–56.
48. Siavashi M, Iranmehr S. Using sharp wedge-shaped porous media in front and wake regions of external nanofluid flow over a bundle of cylinders. Int J Numer Methods Heat Fluid Flow. 2019;29(10):3730–55. https://doi.org/10.1108/HFF-10-2018-0575
49. Norouzi A, Siavashi M, Oskouei M. Efficiency enhancement of the parabolic trough solar collector using the rotating absorber tube and nanoparticles. Renew Energy. 2020; 145:569–584.
50. Selimefendigil F, Oztop H. Corrugated conductive partition effects on MHD free convection of CNT-water nanofluid in a cavity. Int J Heat Mass Transf. 2019;129:265–77.
51. Selimefendigil F, Chamkha A. Magnetohydrodynamics mixed convection in a lid-driven cavity having a corrugated bottom wall and filled with a non-Newtonian power-law fluid under the influence of an inclined magnetic field. J Therm Sci Eng Appl. 2016;8(2):1–8.
52. Selimefendigil F, Oztop H. Conjugate mixed convection of nanofluid in a cubic enclosure separated with a conductive plate and having an inner rotating cylinder. Int J Heat Mass Transf. 2019;139:1000–17.
53. Selimefendigil F, Oztop H. Effects of an inner stationary cylinder having an elastic rod-like extension on the mixed convection of CNT-water nanofluid in a three dimensional vented cavity. Int J Heat Mass Transf. 2019;137:650–68.
54. Selimefendigil F, Ismael M, Chamkha A. Mixed convection in superposed nanofluid and porous layers in square enclosure with inner rotating cylinder. Int J Mech Sci. 2017;124–125:95–108.